Experimental evolution of evolvability

Michael Barnett[1], Lena Zeller[1] and Paul B. Rainey[1,2]

[1]Department of Microbial Population Biology, Max Planck Institute for Evolutionary Biology, August-Thienemann Str. 2, 24306 Plön, Germany

[2]Laboratory of Biophysics and Evolution, CBI, ESPCI Paris, Université PSL, CNRS, 75005 Paris, France

Abstract

Capacity to generate adaptive variation can evolve by natural selection. However, the idea that mutation becomes biased toward specific adaptive outcomes is controversial. We report the *de novo* evolution of enhanced evolvability in experimental populations of bacteria. Key to realisation was a lineage-level birth-death dynamic, where lineage success depended upon capacity to mutate between two phenotypic states, each optima in a cycling environment. A set of early mutations caused selection to focus on a single locus that after refinement became highly mutable, facilitating rapid and reliable transitions between states. Subsequent evolution showed lineages with localised hyper-mutability were more likely to acquire secondary adaptive mutations. Our results provide a detailed mechanistic account of the adaptive evolution of evolvability.

Introduction

The capacity to generate and maintain adaptive phenotypic variation can be shaped by natural selection. Direct evidence comes from experimental studies of evolution in bacteria where mutants with elevated mutation rates are favoured by selection because of increased likelihood of finding beneficial variants [52, 25, 1, 34, 55]. Evolvability in this sense is readily understood. Less clear, and often controversial, is whether (and how) internal organismal features might be shaped by selection such that variability becomes biased toward particular outcomes [53, 45].

One reason for scepticism stems from the fact that natural selection amplifies traits beneficial in the present environment and is 'blind' to future contingencies [53]. Thus the suggestion that selection might structure organisms to evolve in directions *that facilitate future adaptation* is problematic. And yet, environmental change can exhibit regularities over evolutionary timescales that, in theory, might lead to biases in patterns of variability. Indeed, *in silico* evolving populations experiencing selection toward varying and recurring goals, improve capacity to reach these goals over time [11, 29, 8, 7, 18]. They do so by evolving genotype-phenotype mappings in which states adaptive in the past become more readily generated by mutation in the future. Should future selective environments resemble past ones, derived types become biased toward generating adaptive change.

A compelling case for evolvability in this sense is found in the so-called "contingency loci" of pathogenic bacteria [40]. These loci are characterised by the presence of mutation-prone sequences, such as short-sequence repeats, located in promoter regions or in open reading frames of genes, which encode products determining interactions with the external environment. Being prone to slipped-strand mispairing [35], contingency loci mutate at high frequency, causing descendant cells to achieve a diverse, yet biased set of phenotypic states, central to persistence in the face of challenges presented by host immune responses [3].

While a history of repeated encounters with a selective environment dispels any mystery of foresight, traits such as contingency loci, remain difficult to explain without invoking selection at levels above the individual, which is considered weak [53, 39, 60]. This weakness means the kind of cumulative refinement required to generate adaptations is not expected at levels above the individual. However, the logic of natural selection is indifferent to level of organization or timescale, and provided there exists variation, reproduction and heredity, selection will operate [36]. In particular, selection acting on lineages provides opportunity for evolving evolvability [14, 30, 57, 19, 50, 9]: if capacity to generate adaptive variation is limited, then lineages, no matter how well-adapted to the present, are susceptible to extinction on change of environment. Conversely, lineages adept at generating adaptive variation

are likely to persist in the face of change, with opportunity provided to expand and further diversify.

Here, recognising the significance of lineages as units of selection, we asked whether lineage-level selection, in which those lineages better able to generate the next phenotypic state in a repeating cycle replaced those less able, would lead to specific adaptations enhancing evolvability. In one metapopulation, following more than 40 sequential transitions, we observed the *de novo* evolution of local hyper-mutability, precisely analogous to the contingency loci pathogenic bacteria. Of crucial importance was a set of general potentiating mutations that focused selection toward a single regulatory gene, *pflu0185,* followed by a sequence of 24 successive mutations in this single gene, which alternately activated and inactivated gene function. En route, mutations in the promoter region caused transcription to increase, which correlated with an increase in the rate of frame-shifting, ultimately facilitating reliable phenotypic reversals via expansion and contraction of a specific heptanucleotide (HN) sequence. We demonstrate that the derived locus itself is evolutionarily responsive, with copies of the HN-sequence increasing in a predictable manner in response to stringent selection. Finally, we report an unanticipated consequence of contingency behaviour, namely, that lineages with localised hyper-mutability are more likely to acquire secondary adaptive mutations that improve general ecological performance.

Main

The bacterium *Pseudomonas fluorescens* diversifies in spatially structured microcosms [47]. Two niche specialist mutants, the mat-forming cellulose-over-producing (CEL^+) and the mat-colonising non-cellulose producing (CEL^-) types, cycle as a consequence of negative frequency-dependent interactions [46]. Such interactions make possible an experiment in which competing lineages are rewarded for capacity to repeatedly transition between two phenotypic states by mutation. Lineages that fail to generate the target state are replaced by extant lineages (Figure 1).

Evolution of lineages

The selective regime shown in Figure 1 imposes constraints [5] that cause lineages to function as units of selection [36]. While the experiment began with a single genotype in each of the four metapopulations, mutation ensures that by the first phenotypic transition, lineages vary one to another. Failure of lineages to produce the next phenotype in the cyclical series results in extinction, with death providing opportunity for extant lineages to export their evolutionary success, including their evolutionary potential. Because each consecutive stage is founded by a single colony, offspring lineages resemble parental types. Selection thus works over two timescales: the doubling time of cells, and the

doubling time of lineages. Over the long-term, successful lineages stand to be those composed of cells that enhance lineage-level evolvability, with opportunity for cumulative refinement by selection.

Knowledge of the fate of lineages within meta-populations allows precise depiction of evolutionary dynamics (Figure 2). Evident are instances in three of the four meta-populations (A-C) in which descendants of single lineages went to fixation, forming unbroken series of successful transitions. Meta-population D suffered a mass extinction at transition 48. If lineages had not been treated as units of selection, that is, if in the face of extinction, reproduction of lineages had been disallowed, then all meta-populations would all have faced early extinction (Supplementary Figure 1). That selection acts on both viability and fecundity is crucial: in absence of the latter, there is minimal opportunity for exploration of genetic (and thus phenotypic) space, or for refinement of traits.

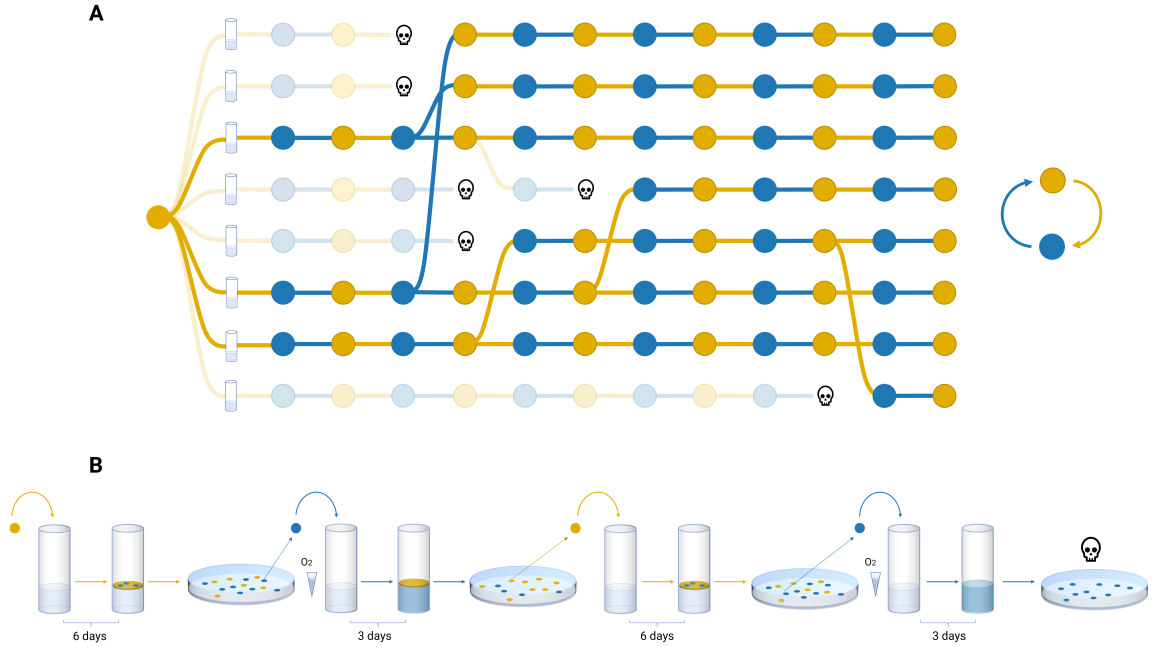

Figure 1: **Lineage selection**. **A.** Graphical representation of the experimental regime depicting eight competing lineages founded from a single common genotype. Lineages are required to transition repeatedly between CEL$^+$(yellow) and CEL$^-$(blue) states by mutation. Lineages that fail to achieve the target phenotype are marked extinct, with extinction providing opportunity for extant lineages to export their evolutionary success. **B.** Schematic of protocol that begins by founding a microcosm with a single CEL$^+$ genotype. After six days in static culture, descendant cells are diluted and plated on agar with colony phenotype allowing detection of CEL$^-$ mutants. A single CEL$^-$ mutant is then used to found growth in a fresh microcosm, with a sample again examined by agar plate culture for the presence of CEL$^+$ types. A single CEL$^+$ type then founds the next bout of selection and the cycle repeats. The illustrated lineage goes extinct on the final transfer because it failed to generate the next (CEL$^+$) target phenotype. Key to the selection regime are frequency-dependent interactions between CEL$^+$ and CEL$^-$: CEL$^+$ forms a mat at the surface and provides conditions that favour CEL$^-$ mutants; CEL$^-$ types deplete oxygen thus establishing conditions that favour the evolution of surface-colonising CEL$^+$ types. Photos are shown in Figure 3E.

Whole genome sequence of derived lineages from meta-populations A-C were obtained at the end point of each series, but also periodically en route. In meta-populations A and C, lineages carrying loss-of-function (LoF) mutations in genes involved in mutational repair fixed (*mutS* and *uvrD*, respectively), with the point of origin marked in Figure 2. In contrast, no mutations affecting genes involved in DNA replication or repair were detected in the derived lineages of meta-population B, prompting continuation of the experiment.

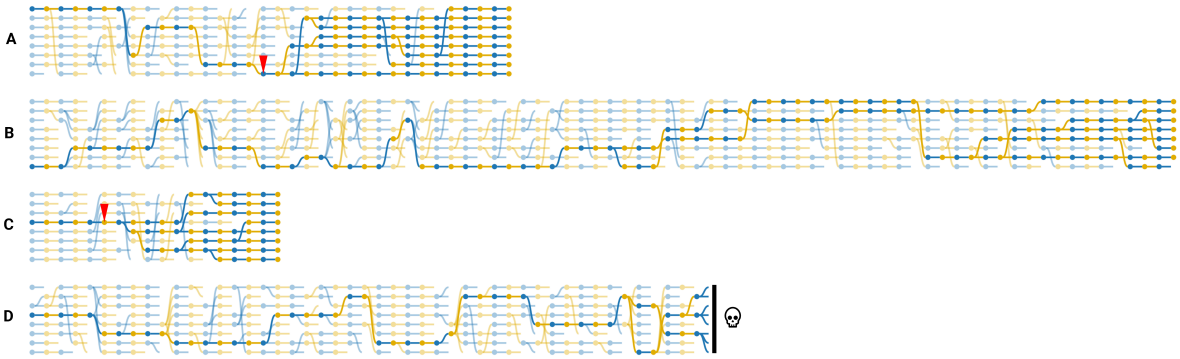

Figure 2: **Evolutionary dynamics of meta-populations**. Four CEL$^+$ genotypes were used to found each of four meta-populations (A-D) each composed of eight lineages. yellow nodes indicate the CEL$^+$ target phenotype and blue, CEL$^-$. Lineage death occurred through failure to generate the target phenotype and provided extant lineages opportunity for birth. Solid lines depict the genealogy of final surviving lineages, with extinctions indicated by broken faded lines. Red arrows in A and C indicate the point of origin of mutator genotypes founding lineages that rapidly fixed (see text).

Meta-population B ultimately cycled through 80 transitions (720 days within microcosms) with the experiment being terminated on evidence of gradual fixation of a single lineage. This meta-population experienced 120 lineage deaths and subsequent births. Fluctuation assays (based on resistance to rifampicin) of representative genotypes from derived lineages showed that global rates of mutation among lineages from meta-populations A and C were elevated 300-fold and 350-fold, respectively, however the mutation rate among derived lineages of meta-populations B and D did not differ from ancestral *P. fluorescens* SBW25 (Supplementary Figure 2).

Local hyper-mutability underpins lineage adaptation

To understand the mutational history and genetic bases of both successful and unsuccessful lineages whole-genome re-sequencing was used to identify and order of mutations underpinning transitions between CEL$^+$ and CEL$^-$ states. This revealed 548 mutational events that targeted 84 genes, 34 of which were hit multiple times. Despite the availability of diverse mutational paths, a single regulatory gene, *pflu0185*, became the main mutational target, eventually accounting for 59% (306 of 520) of all phenotypic transitions (Figure 3). Moreover, the majority of these (186 of 306) were caused by

duplication and loss of a single heptanucleotide (HN)-sequence 'GGTGCCC' located near the 5' end of the gene (nucleotides 19-25). Mapping the occurrence of phenotypic transitions effected by changes in copy number of the HN-sequence on dynamics of lineages within meta population B (Figure 3C) showed that transitions involving gain and loss of the HN-sequence were associated with a decrease in the number of extinctions from 26% per transition to 10% (Figure 3A).

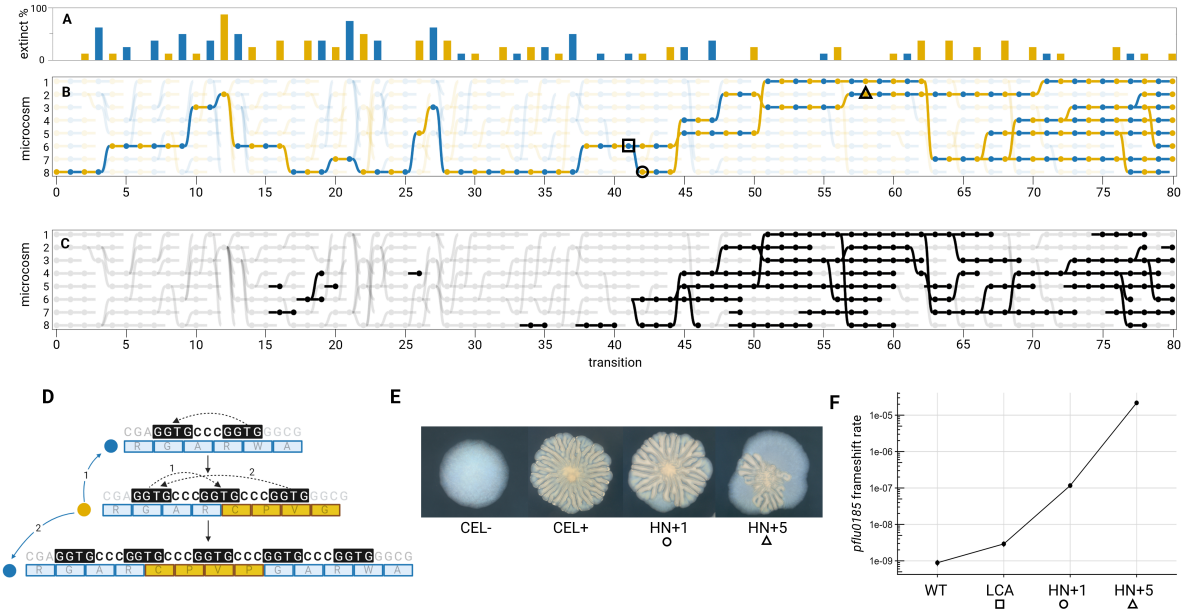

Figure 3: **Local hyper-mutability accounts for adaptive advantage of derived lineages in meta-population B**. **A**. Extinction events at CEL$^+$ (yellow) and CEL$^-$ (blue) transitions. **B**. Lineage dynamics with focal points indicated by symbols around nodes (see text). X-axis labels are transitions (T) and Y-axes denotes microcosm (M). The node identified by the square box is thus T41 M6. **C**. Phenotypic transitions effected by changes in the number of copies of a HN-sequence in *pflu0185*. **D**. Proposed mechanism of slipped-strand mispairing. Top shows the DNA sequence of *pflu0185* surrounding, and including, the focal HN-sequence (GGTGCCC) plus relevant downstream nucleotides (GGTG). The dotted arrow indicates mispairing between GGTG repeats which leads to an additional copy of the HN-sequence (middle, vertical arrow). With two copies of the HN-sequence the reading frame is destroyed. The reading frame can be corrected by either mispairing in the forward direction (dotted arrow 1), which restores the original state (blue arrow 1); or, mispairing in the reverse direction (dotted arrow 2) resulting in four copies of the HN-sequence (bottom, vertical arrow). **E**. Image of CEL$^-$ and CEL$^+$ colonies following prolonged (72 h) growth on agar plates with derived lineages having either a single additional copy of the HN-sequence, or five additional copies – the latter showing overt sectoring indicative of an elevated mutation rate. **F**. Relationship between genotype and rate of frame-shift mutations in *pflu0185* determined by fluctuation assay. Symbols denote genotypes from (B). Error bars (largely contained within the points) are 95% CI.

Pflu0185 is a regulatory protein composed of two enzymatic domains: a diguanylate cyclase (DGC) — responsible for the synthesis of cyclic-di-GMP (c-di-GMP) — and a phosphodiesterase (PDE) — responsible for breakdown of c-di-GMP [49]. In *P. aeruginosa* functional analysis shows the protein to have PDE function, but no DGC activity [6]. This is consistent with the genetic analysis reported here. The cellulose biosynthetic *wss* operon is allosterically activated by c-di-GMP, such that when

levels are elevated the CEL$^+$ state is achieved, but when reduced, cells areCEL$^-$[54]. With just a single copy of the HN-sequence, PDE function is intact, c-di-GMP levels are low and cells realise the CEL$^-$ state. On addition of an extra copy of the HN-sequence the reading frame is destroyed, PDE function is lost, c-di-GMP levels increase, and cells become CEL$^+$.

Mechanistically, rapid changes in the number of copies of short sequence repeats can be attributed to slipped-strand mispairing — a genomic instability that increases the likelihood of deleting or duplicating repeated units [35]. Relevant here is the fact that downstream of the duplicated HNsequence (GGTGCCC) is a further copy of GGTG and thus the focal sequence is GGTGcccGGTG (Figure 3D). Mis-pairing between the two copies of GGTG stand to catalyse a duplication event that is readily reversible by forward slippage. However, with one additional copy of the HN-sequence (three copies of GGTG), reverse slippage results in two further copies of the HN-sequence and restores the reading frame (Figure 3D).

Once in the CEL$^+$ state (one additional copy of the HN-sequence), 96% of lineages inheriting the duplication reactivated Pflu0185 in the next transition through correction of the reading-frame, and were ∼eight times more likely to survive the next transition compared to inheritance of any other regulatory mutation (95% CI [2.5, 26], P=0.0002, Fisher's exact test, two-tailed). Of lineages that achieved the two-copy (non-functional) state, 86 of 89 instances involved restoration of the *pflu0185* reading frame by contraction. In three instances the reading frame was restored by expansion of the tract through addition of two copies. Such lineages were more likely to see further increase in copy number of the HN-sequence at the next transition (5:3 contraction:expansion, P=0.0049, Fisher's exact test, two-tailed). As the number of repeats increased, the rate at which transitions occurred visibly increased (Figure 3E).

By T41 M6 (black square in Figure 3B) duplication of the HN-sequence became increasingly probable even in the face of numerous additional paths for generating LoF mutations — both within *pflu0185* and elsewhere in the genome. Indeed, alternative LoF mutations in *pflu0185* were occasionally observed late in evolution and, where irreparable, led to lineage extinction (Supplementary Figure S3A).

The relationship between number of tandem repeats and rate at which phenotypic variants are generated [15] predicts that as copy number increases, so too will local mutation rate. While global measures of mutation rate reported above showed no increase, by translationally fusing *pflu0185* to an out-of-frame kanamycin resistance (*kanR*) gene, the rate of frame-shifting, specifically within *pflu0185*, could be assessed by fluctuation assay (Figure 3F). Surprisingly, a statistically significant three-fold increase in the rate of frame-shifting was evident in the genotype that marked the coalescent point of the final lineages (T41 M6 (LCA), black square in Figure 3B), despite the fact that this genotype carried no additional copy of the HN-sequence. With two copies ((T42 M8), black circle in Figure 3A), the rate of frame-shifting increased a further 150-fold, and with six (+5) copies (T58 M2, black triangle in Figure 3B) (the maximum observed in the selection experiment) the rate of frame-shifting was more than four orders of magnitude greater than the ancestral genotype (Figure 3F).

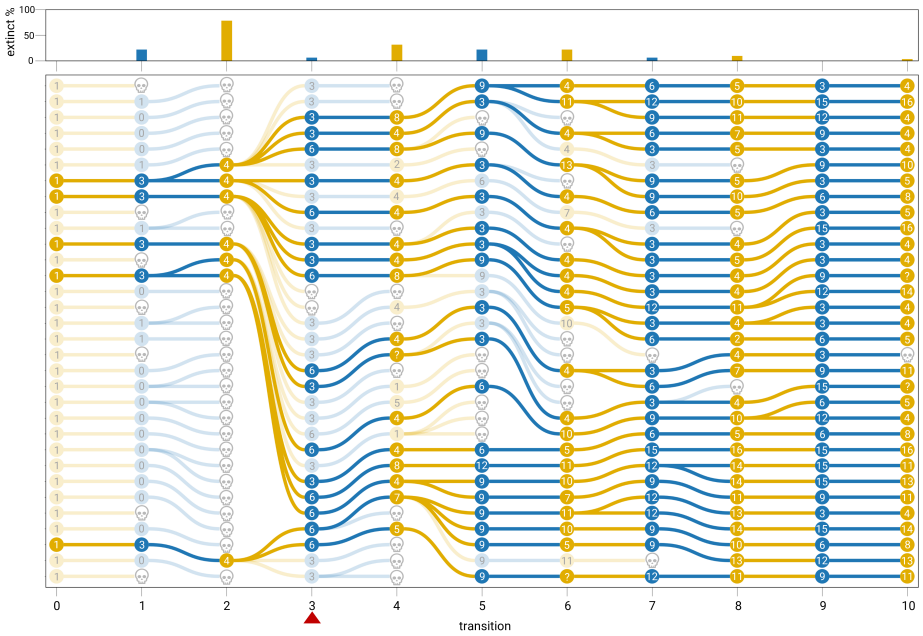

Figure 4: **Stringent selection drives expansion in HN copy number**. A total of 32 lineages were founded by genotype T42 M8 (black circle in Figure 3B) containing a single additional copy of the HN-sequence. Lineages were subject to the selection regime as shown in Figure 1, but population size was reduced 30-fold and lineages were required to achieve the target phenotype within 24 hours or face extinction. The number of additional HN units over the ancestral SBW25 *pflu0185* sequence is indicated within nodes. Colour code for phenotypic states are as described previously. The red triangle indicates a point after which the stringency of selection was further increased by requiring successful lineages to have at least five colonies of the target phenotype present. The upper panel shows extinctions at each transition.

Despite the evident potential for self-accelerating increases in mutation rate by successive extension of repeats, all lineages that expanded the HNsequence periodically reverted to a single copy. We reasoned that this tendency was a consequence of mutation supply (population size and propagation time), which meant extreme mutation rates (Figure 3F) were not necessary to reliably generate cells with

the target phenotype. Accordingly, we took a single CEL$^+$ genotype carrying the initial HN-duplication (+1 GGTGCCC unit) (T42 M8 black circle in Figure 3B) and used this genotype to found 32 lineages that competed under a restrictive regime where population size was reduced by a factor of thirty and persistence required re-establishment of the target state every 24 h (Figure 4).

The selective response, lineage-level dynamics, and changes in numbers of repeats over ten transitions are revealing. Most lineages managed — within 24 h — to achieve the CEL$^-$ state required for the first transition, but the majority did so by losing one copy of the HN-sequence. Without exception, those lineages that switched to CEL$^-$ by loss, were unable to transition to the CEL$^+$ state during the next 24 h period and thus went extinct. In sharp contrast, those lineages that achieved the CEL$^-$ state (at transition 1) by adding three additional copies, became progenitors of lineages that persisted throughout the course of the experiment. At the end point, lineages harboured on average 8 additional copies of the HN-sequence, with some acquiring as many as 16. A clear association is evident between the number of copies of the HN-sequence and likelihood of survival (Figure 4).

Navigating multiple paths and avoiding genetic dead-ends

Having observed the *de novo* evolution of localised adaptive hyper-mutability, we next sought understanding of its evolutionary origins. Genome sequence data showed that the majority (89%) of phenotypic transitions were associated with single mutations, allowing the causes of transitions to be precisely identified.

The switch between CEL$^-$ and CEL$^+$ states is asymmetrical with details of the genetic architecture of components affecting cellulose production being described in Figure 5A. Figures 5B-D provide a visual representation of principle changes for all lineages from meta-population B at three different transition stages. The full data set is available via an interactive website (micropop.evolbio.mpg.de/data/evolve) and Supplementary Video 1 allows sequential accumulation of mutations and genetic targets (up to T41) for all lineages of meta-population B to be viewed transition-by-transition.

Figure 5B displays mutational history at transition T6 and shows mutations in a range of genes, most of which are positive regulators of cellulose biosynthesis (DGCs, green squares), and one of which, the DGC-encoding *awsR*, was targeted by mutation multiple times, effecting repeated transitions between CEL$^-$ and CEL$^+$ (self-loop circling *awsR*). By transition T13 (Figure 5C), an increasing number of transitions were triggered by further cycles of mutation targeting *awsR*, however, utility of *awsR* ceased upon occurrence of a 54 base pair deletion at T9 M6, which fixed within the meta-population at transition 12, following an almost fatal extinction event. Additionally, the diversity of mutational

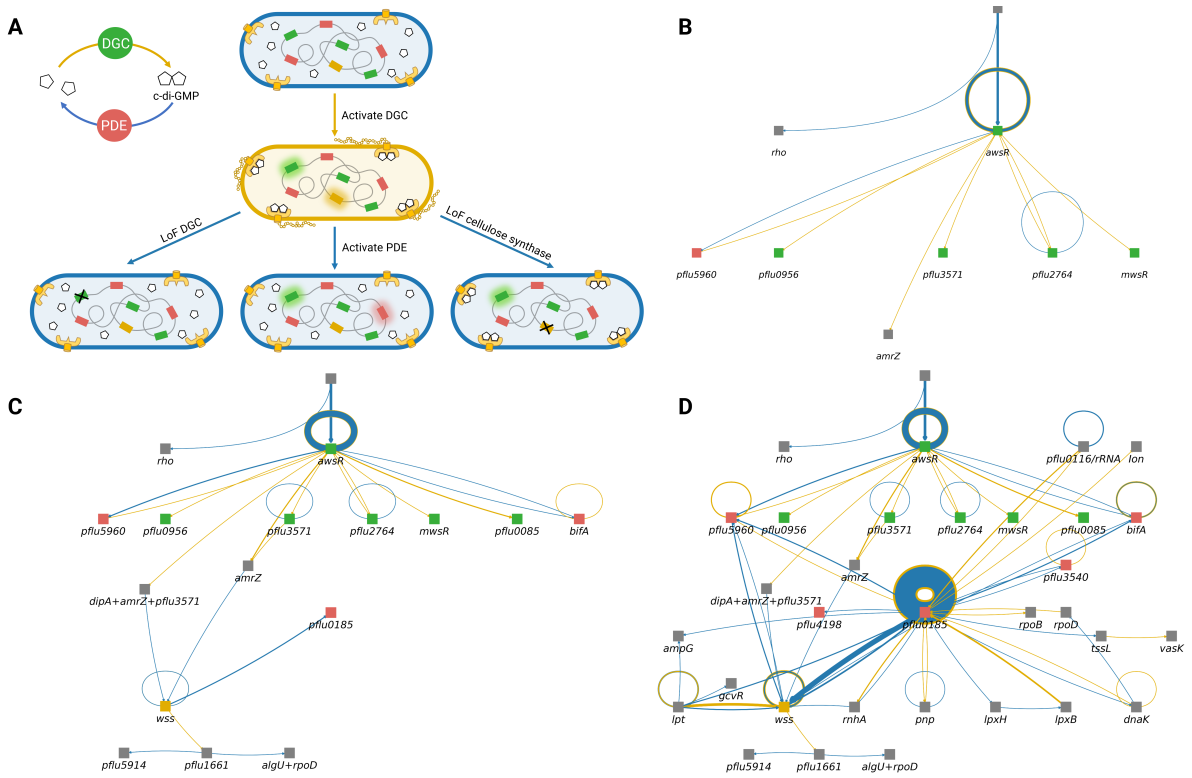

Figure 5: **Diversity of mutational paths generating variation in evolutionary potential**. **A**. Genetic architecture underpinning mutational transitions between CEL$^-$ and CEL$^+$states. C-di-GMP is the critical signalling molecule and allosteric activator of cellulose synthesis. The molecule is synthesised from two molecules of guanosine-5'-triphosphate (GTP) (diamond symbols) by diguanylate cyclases (DGCs) and degraded by phosphodiesterases (PDEs), which function as positive and negative regulators, respectively. Red boxes in cells denote genes encoding PDEs, green boxes depict DGCs and the yellow box is the structural determinant of cellulose encoded by the 10 gene *wss* operon. The CEL$^+$ state is realised by mutations that elevate c-di-GMP levels. Once in the CEL$^+$ state, there exist three primary routes to CEL$^-$: mutational inactivation of DGCs, mutational activation of PDEs, or LoF mutations in cellulose synthesis. The SBW25 genome encodes 41 genes with roles in synthesis and degradation of c-di-GMP, with 394 of the 548 mutations identified within (or adjacent to) genes involved in modulation of c-di-GMP levels. **B-D**. Snap shots of mutational trajectories at transition T6 (B), T13 (C) and T41 (D) for all lineages from meta-population B starting from the ancestral state (the CEL$^+$ genotype used to found all eight lineages). The full sequence is available as a video (Supplementary Video 1). Lines indicate successive sequences of genetic targets (boxes). Line thickness indicates the frequency with which the mutational route was used. Blue lines indicate transitions from CEL$^+$ to CEL$^-$ and yellow lines from CEL$^-$ to CEL$^+$ as in Figure 5A. The yellow box depicts the cellulose synthesis encoding machinery. Self-loops, for example around *awsR* in C, and around *pflu0185* in D, indicate repeated transitions via successive activating/inactivating mutations at these loci.

routes further expanded with many, including mutations in the cellulose synthesis operon, *wss*, proving dead-ends. Mutations that generate CEL$^-$ through destruction of the cellulose biosynthetic machinery accounted for 16% of all transitions, with these lineages being ∼10 times more likely to go extinct at the next transition compared to any other target (P<0.0001, Fisher's exact test, two-tailed). This stems from the fact that cellulose synthesis is essential for the CEL$^+$ phenotype, thus LoF mutations must be repaired at the next transition in order to avoid extinction.

In contrast to extinction events arising from mutations within the structural *wss* locus, numerous genes controlling c-di-GMP levels provided opportunity for mutation to successively activate and inactivate cellulose biosynthesis via multiple redundant targets (Figure 5C). Additional flexibility was evident in individual regulatory genes. For example, LoF caused by substitutions were often compensated by changes at residues elsewhere in the same regulatory gene (or through mutations in the 5'-untranslated region that likely increased gene expression). In contrast, not a single such instance was observed for the structural locus (*wss*), where repair came about almost exclusively through direct reversions (Supplementary Table 1). This indicates a much tighter structure-function relationship for the *wss* locus, contributing to this target being a frequent dead-end.

Also notable at transition T13 (Figure 5C) are mutations that target negative regulators of cellulose biosynthesis (PDEs, red squares), with an unusual sequence of mutations bringing the PDE activity of *plu0185* into play. At T10 M3, in the lineage that went to fixation, three atypical mutations co-occurred. These targeted genes encoding a PDE (*dipA*), a DGC (*pflu3571*) and the global transcriptional regulator *amrZ*. The latter is conserved across *Pseudomonas* where it controls transcription of multiple DGCs [42]. We hypothesized this unusual triple-mutant path had caused the source of cyclic-di-GMP to become distributed across multiple DGC-encoding loci, such that LoF mutations at any single DGC, were no longer able to reduce c-di-GMP levels sufficient to generate the CEL$^-$ state. In support of this hypothesis, transposon mutagenesis was employed in an attempt to identify genes capable of suppressing the phenotype of CEL$^+$ at transition 10 (M3), but no DGC-encoding loci were identified. Assuming a Poisson distribution of transposon insertions across the SBW25 genome (6,700 genes), the probability of a gene remaining undetected given our screen of 54,000 mutants is $\sim$0.0003.

From transition 14 onward, successful lineages no longer generated CEL$^-$ via changes in DGCs, but did so instead by mutations that affected the activity of PDEs (Supplementary Figure 4). The sudden switch from positive regulators (DGCs) as mutational targets to negative regulators (PDEs) was unexpected, as numerous other intact DGC-encoding genes capable of generating CEL$^+$ through single mutations are known [38]. The shift from DGCs as targets, to PDEs, marked a significant contraction in the range of mutational targets and was instrumental in turning the focus of selection to negative regulators and increasingly to *pflu0185*.

Figure 5D depicts mutational history of all lineages up to transition 41, the coalescence point of the surviving lineages and moment where transitions between CEL$^+$ and CEL$^-$ were often underpinned by changes in copy number of the HNrepeat (Figure 3C). Evident are a diversity of one-off mutational routes, the majority of which proved evolutionary dead-ends. Striking, however, is the fact that *pflu0185* became the target of multiple mutations that facilitated repeated switching between CEL$^+$

and CEL$^-$ states (thick self-loop circling *pflu0185*). Supplementary Figures 3A-C detail mutational histories of three sub-lineages highlighting particularly fascinating examples of how each mutation opened and closed potential evolutionary paths.

Concomitant increases in transcription and mutation rate at *pflu0185* potentiated repeat-associated hyper-mutation

The series of mutations targeting *pflu0185* that occurred in the focal lineage up to T41 M6 (Figure 3B) are detailed in Figure 6A. Each mutation was responsible for the transition between CEL$^+$ and CEL$^-$ states via effects on the PDE activity of *pflu0185*. At the point of coalescence (T41, M6) *pflu0185* had acquired 24 mutations (including three direct reversals), either within, or upstream of the gene. Among this convoluted history of mutations, no single event stood out in terms of relevance to hyper-mutability caused by changes in copy number of the HN-sequence. However, given a three-fold increase in mutation rate at T41 M6 (compared to ancestral SBW25) (Figure 3F), combined with the presence of multiple mutations in the upstream region, and recognising the mutagenic nature of transcription [13], attention turned to the effect of selected mutations on the rate of frame-shifting within *pflu0185*. This was achieved by fluctuation assay using the translational *pflu0185-kanR* gene fusion.

However, before measuring changes in the rate of frame-shifting we first took advantage of the gene fusion to measure the effects of selected mutations on transcription, particularly those occurring upstream of the *pflu0185*open reading frame (Figure 6B). This revealed a ratcheting effect of mutations, with those causing either a reduction in transcription of *pflu0185*, or reduction in PDE activity (leading to the CEL$^+$ state), being compensated for by mutations in the upstream region that elevated transcription (leading to the CEL$^-$ state). By the end of this series of mutations (Figure 6B) transcription of *pflu0185* was elevated 30-fold above that of ancestral SBW25.

We next asked whether upstream mutations might have contributed to formation of recognisable promoter motifs. Changes, documented in Figure 6C, and placed in context of surrounding nucleotides, deliver a promoter sequence typical of those found in *Pseudomonas* [17, 56]. Such mutational changes are consistent with the measured elevation in MIC being caused by transcriptional changes.

In terms of the possibility that these mutations might have potentiated proclivity of the HN-sequence to expand in copy number, the relationship between MIC and rate of frameshift mutations in *pflu0185* was determined by fluctuation assay (Figure 6D). The results show that the −169 C→T mutation produced a highly significant two-fold increase in the rate of frameshifting compared to ancestral (wildtype) *P. fluorescens* SBW25. This was further increased by mutation Q500P (T41 M6) that mark

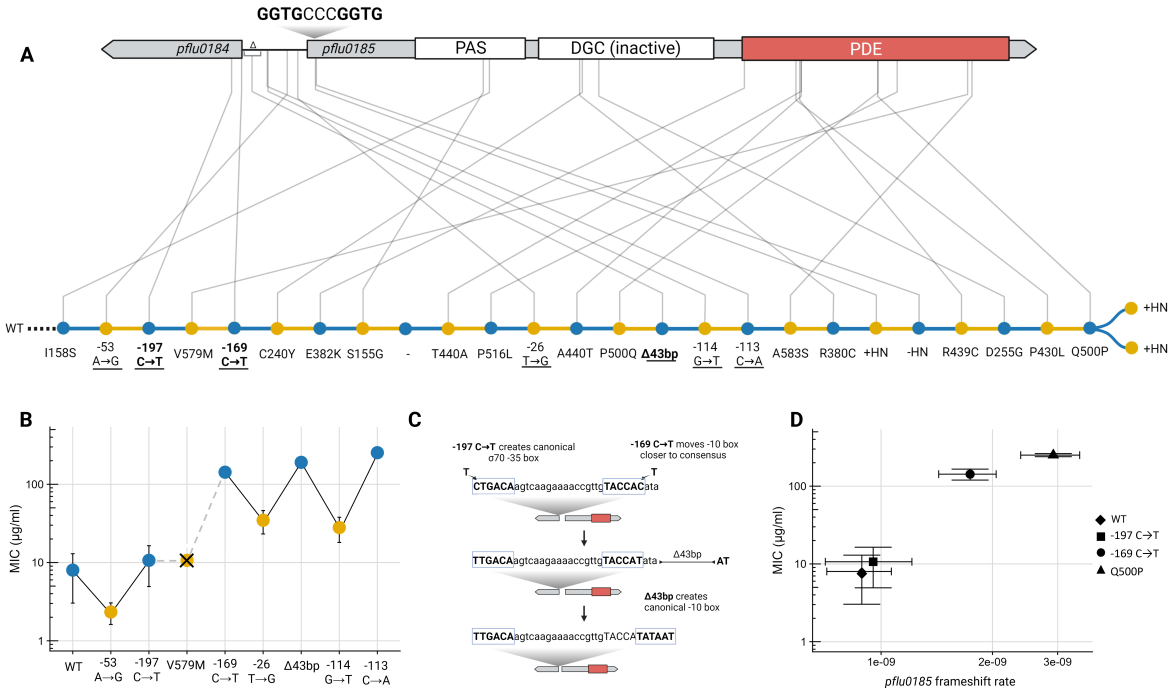

Figure 6: **Mutational history of potentiating mutations in *pflu0185*.A**. Genetic structure of *pflu0185* and sequence of successive mutations modulating changes in phenotypic state. The top portion of A shows the *pflu0185* open reading frame with location of the HN-sequence, PAS signalling domain, inactive DGC domain and, in red, the PDE domain. Also shown is the upstream gene and intergenic space where multiple mutations arose that affected transcription. **B**. Effects of mutations on transcription of *pflu0185* and CEL$^+$/ CEL$^-$ status determined through assay of MIC in the presence of kanamycin (putative promoter mutations are underlined in A). The first mutation upstream of *pflu0185*(−53 A→G) (which generated the CEL$^+$ phenotype), led to a four-fold reduction in MIC compared to ancestral SBW25. The next mutation (−197 C→T), also in the upstream region, caused CEL$^+$ to switch to CEL$^-$ by restoring PDE activity via changes to expression that returned the MIC to that of the ancestral type. The following transition, from CEL$^-$ to CEL$^+$, occurred via intragenic mutation within the PDE domain (V579M), resulting in reduction of activity sufficient to allow c-di-GMP levels to rise to a level that triggered the CEL$^+$ state. The next transition (to CEL$^-$) occurred, once again, via an upstream mutation (−167 C→T), which caused a further ten-fold increase in MIC sufficient to compensate for the previous reduction in PDE activity. Following the −167 C→T mutation were a series of changes in the open reading frame of *pflu0185*, punctuated by four further upstream mutations, with the last of these (−113 C→A) achieving a 30-fold increase in MIC over the ancestral level. Mutation V579M is included to demonstrate its role in reducing catalytic activity of the PDE, necessitating further increases in *pflu0185* transcription. **C**. Mutational changes in upstream regions (in bold type) placed in context of surrounding DNA sequence that contribute to formation of a typical *Pseudomonas* promoter. **D**. Relationship between transcription (as determined by MIC assay) and rate of frame-shift mutations in *pflu0185*. Note that the MIC of Q500P is equivalent to the last upstream mutation (−133 C→A). Error bars are 95% CIs

.

the coalescent point of the final lineages (following which transitions via the HN-sequence dominated) and whose genotype includes the final −113 C→A mutation that led to maximal expression of *pflu0185*.

Localised hyper-mutability of *pflu0185*-facilitated additional adaptive evolution

A final observation concerns transitions between CEL$^+$ and CEL$^-$ associated with multiple mutations. Those transitions effected by changes in HN-repeat number were more than three times as likely to be associated with additional (secondary) mutations. Of 91 such transitions, 19 harboured secondary mutations (21%). In contrast, of 167 transitions effected by mutations not involving the HN-sequence, only 10 carried secondary mutations (6%) (P=0.0007, Fisher's exact test, two-tailed).

While secondary mutations that hitchhike with transition-causing mutations are to be expected (Supplementary Table 2), mutations in loci encoding genes connected to chemotaxis and motility (Supplementary Table 3), have conceivable ecological relevance. Moreover, two loci, the aerotaxis receptor *aer* (*pflu4551*) and a methyl-accepting chemotaxis protein (*pflu1687*), were observed to occur repeatedly (six and four times, respectively) across multiple lineages during transitions mediated by the HN-sequence (Figure 7A). Such striking parallelism suggested these mutations were themselves adaptive. Figure 7B elaborates the benefit presumed to accrue to lineages derived from genotypes that switch phenotype early, and reliably.

To test the adaptive hypothesis, the fitness effects of a sample of mutations were determined relative to immediate ancestral types, both in CEL$^+$ and CEL$^-$ backgrounds (Figure 7C). With emphasis on the lineage that descends from T42 M6, the first mutation examined (in T43 M6) was in FleQ (R371C), a master regulator of motility and polysaccharide production (including cellulose) [26, 22]. Relative to the immediate ancestral types the *fleQ* mutation increased fitness ∼10% in CEL$^+$, but marginally decreased fitness in CEL$^-$. The next mutation, in FleN (L42Q) (T58 M1), which also regulates flagella through interactions with FleQ [12], increased fitness of CEL$^+$ by a further ∼30%, with minimal effects in CEL$^-$. Relative to the fitness of T42, M6, the two mutations combined contributed a ∼40% fitness gain in CEL$^+$.

The genotype at T62 M7 carries two additional mutations (one of only three instances in the experiment where three mutations occurred at the same transition), one a 21 base pair deletion in Aer and the other a stop codon within FimV (Q640*). These two mutations reduced fitness of CEL$^+$ by ∼10%, while increasing fitness of CEL$^-$ by ∼5%. With the exception of Pflu1687 (S6N) in the CEL$^+$ state, no further fitness effects were detected. Secondary mutations in other lineages were also examined, including changes in the chemotaxis protein CheB (T92P at T53 M6) and further mutations in Aer (S260P at T60 M2 and Δ9bp at T62 M1), with the largest contribution coming from Aer S260P in the CEL$^-$ state). Together the range of effects shown in Figure 7C are consistent with the hypothesis

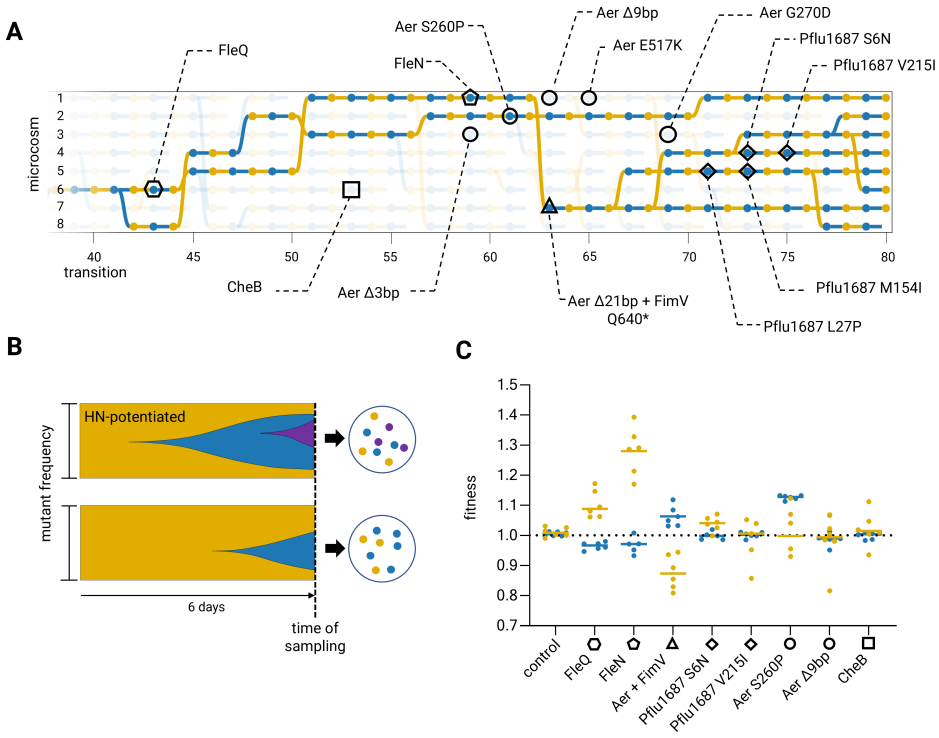

Figure 7: **Secondary mutations and fitness effects**. **A**. Genealogy of successful lineages from meta-population B between transition 40 and 80 on which secondary mutations of predicted ecological significance are indicated. **B**. Muller plots showing predicted consequences of presence (top) and absence (bottom) of local hyper-mutation: early and reliable switching provides enhanced opportunity for secondary mutations (purple) to reach high frequency (top). **C**. Fitness consequences of mutations determined by competitive assay against immediate ancestral types in CEL$^+$(yellow) and CEL$^-$(blue) backgrounds. Lines indicate mean value.

that at least some secondary mutations co-occurring with changes in HN-repeat number are adaptive.

Discussion

Evolution by natural selection is a blind process, but living systems can appear endowed with evolutionary foresight [14, 27]. Mechanistically, this is conceivable. Certain configurations of gene regulatory networks [58, 11, 59], developmental systems [30], chromosomal architectures [8, 44], and mutational processes [40, 23] have apparent adaptive utility in future environments. Ability to realise such advantages requires not only memory of past history, but often an ability to regenerate previously achieved phenotypic states — akin to gene regulation, but over evolutionary timescales. Here we have detailed how selection on lineages can incorporate prior evolutionary history into the genetic architecture of a single cell such that mutation appears to anticipate future environmental change.

Central to our findings was a selective process where lineages better able to generate, by mutation, adaptive phenotypic variation, replaced those that were less proficient (Figure 1). Of the four original

meta-populations (Figure 2), one went extinct, two evolved global hyper-mutators, but in the fourth, a single lineage emerged with capacity to switch rapidly between phenotypic states via expansion and contraction of a short nucleotide repeat in a manner precisely analogous to that of contingency loci in pathogenic bacteria [40]. Moreover, when multiple lineages of a single genotype carrying the mutational history of 42 previous transitions, but carrying just a single additional copy of the HN-sequence (T42 M8, Figure 3C), were propagated under a regime that required phenotypic switching on a daily basis, lineages with up to 16 copies of the repeat rapidly emerged (Figure 4). This demonstrates not only capacity of the HN-repeat within *pflu0185* to generate adaptive phenotypic variation but shows that the locus, in its derived state, is itself highly evolvable.

Selection works most forcefully on individuals and is typically weak at higher levels of organisation [39, 60, 53]. In our experiments, the death and birth of lineages established a feedback between lineage-level properties and the evolutionary dynamics of cells. While selection within microcosms favours fast-growing cells, successful lineages were those with capacity to generate phenotypic variants suited to the future environment. Selection over the doubling time of lineages thus served to align cell and lineage fitness, precisely as occurs during, for example, the evolutionary transition from cells to multicellular life [5]. Moreover, adding potency to lineage selection was the fact that, throughout our experiment, variation in evolutionary potential between lineages resulted from how adaptive CEL$^+$ and CEL$^-$ phenotypes were instantiated by mutation. This departs from the common assumption —and basis for doubting the efficacy of selection on evolvability— that mutations altering evolutionary potential deliver no immediate benefit to the organism and are therefore susceptible to loss via drift [39, 53].

Data presented in Figure 4 (and available online) provides an unprecedented view of evolutionary change. Here, the entire mutational history of a single meta-population is evident. Moreover, given knowledge of the genetic architecture underpinning CEL$^+$ and CEL$^-$ states, it has been possible to causally connect hundreds of mutations to their phenotypic consequences. Notable was the shift in mutational targets from DGCs to PDEs, caused by mutations that brought about distributed production of c-di-GMP, and which in turn arose in response to near fatal collapse of meta-population B caused by elimination of *awsR* as a viable mutational path (Figure 5C).

With selection increasingly focusing on PDEs, *pflu0185* was targeted by mutations multiple times, prior to the locus acquiring hyper-mutator status. That a single gene can withstand being repeatedly broken and repaired to the extent shown in Figure 6 is remarkable. While the series of mutations was instrumental in the increasing the likelihood that the HN-sequence within *pflu0185*, none stood out as obvious candidates. However, noting that switches to CEL$^+$, due to mutations in the open reading

frame of *pflu0185*, were often compensated for by mutations in the promoter region, we predicted that mutations in the upstream sequence effected a reduction in c-di-GMP by elevating transcription sufficient to compensate for previously reduced catalytic activity. This indeed proved to be true with repeated interplay between mutations affecting gene function and transcriptional activity eventually elevating transcription ∼15-fold (Figure 6B). Moreover, elevated transcription was associated with significant increases in the rate of local frame-shift mutations. It is this, namely the connection between transcription and frame-shifting, that we suggest was instrumental in enhancing the likelihood that the HN-sequence duplicated. Transcription is known to be mutagenic with transcription-associated mutagenesis [28] and transcription-coupled repair [21] both playing plausible roles.

Observation of additional (secondary) adaptive mutations associated with local hyper-mutation of *pflu0185* led us to reason that increased propensity to switch enhances the possibility that secondary adaptive mutations, which would otherwise be stalled by the waiting time required to achieve the primary transition-mediating mutation, can increase in frequency (Figure 7B). Indeed, data presented in Figure 7 supports this hypothesis showing how evolution can be sped up but without the threat of Muller's ratchet that arises from global hyper mutation [51, 10]: ability to generate adaptive phenotypic variation provides a 'head-start' to adapt to other aspects of the local environment with feedback affecting further lineage success.

Finally, we turn to broader implications of the study and particularly the extent to which findings here might have general relevance. The selective regime employed was contrived, with selection on lineages being strictly enforced. Such stringent conditions are likely limited in nature. However, microbial pathogens faced with the challenge of persistence in face of the host immune response, will experience strong lineage-level selection, with repeated transitions through selective bottlenecks [41]. As we have shown here, precisely these conditions serve to promote the evolution of evolvability. Indeed, that the genomes of obligate pathogenic bacteria are replete with contingency loci bears testimony to this fact. Notably, while each such locus might be constructed through repeated encounters with specific selective environments, possession of multiple loci enables realisation of phenotypic states that stand to enhance evolvability in novel environments (cf. [43]).

But we further suggest that selection on lineages is more important than generally appreciated [24]. Lineages need only differ in evolutionary potential, for example in how adaptive phenotypes are instantiated by mutation. Provided they co-exist for sufficient time that phenotypic consequences manifest, then lineages differing in capacity to generate adaptive variation stand to compete [61, 20, 33]. This will be particularly relevant in situations where transmission / migration involves passage through bottlenecks that require variation to be generated afresh [31, 37, 4]. Moreover, as demonstrated here, if

challenges to lineage survival repeat across time, then adaptations that enhance evolvability— shaped by lineage selection for the benefit of lineages—can be expected.

Materials and Methods

Experimental evolution

Both CEL$^+$ and CEL$^-$ were propagated 25 ml glass microcosms containing 6 ml of King's Medium B (KB) at 28°C, without shaking. The four meta-populations were founded by single genotypes derived from a previous, but conceptually similar, experiment [25]. Founding genotypes carried on average nine unique mutations, primarily in characterized c-di-GMP regulators (Supplementary table 4).

For the CEL$^+$ to CEL$^-$ phase, microcosms were incubated for six days, vortexed, and 50 μl of a 3.35×10^5-fold dilution spread on a KB agar plate. After 48 hours growth each plate was then examined for the presence of CEL$^-$ colonies, with a single colony used to inoculate a fresh microcosm and initiate a three day growth period. 100 μl of an 8.0×10^6-fold dilution of each microcosm was plated and screened for CEL$^+$ types. The process was iterated. A random number generator was used to determine the extant lineage that would replace extinct lineages. When an entire meta-population failed to generate the target state twice over, propagation was ceased (as in meta-population D).

The births and deaths of lineages were recorded, and the resulting lineage dynamics visualized using Colgen (gitlab.com/ecoevomath/colgen). Overnight cultures of each selected CEL$^-$ and CEL$^+$ colony were stored at -80°C in 33% glycerol saline. The 'stringent selection' experiment followed the same procedure as above but with cells evolved in 96-well plates containing 200μl of KB, and a reduced period of 24 hours given before dilution and screening.

Sequencing and detection of mutations

Visualization and knowledge of genealogy was used to inform both whole-genome re-sequencing and targeted Sanger sequencing to detect and order mutational events. For meta-population B, 482 clones representing successive time-points of the experiment were sequenced, allowing precise ordering of mutations underpinning the majority of the 520 transitions. Remaining transitions and associated mutations were then inferred by parsimony or confirmed by Sanger sequencing. In one instance, to resolve an ambiguity, a mutation (-197 C→T *pflu1085*) was re-constructed to confirm its phenotypic effect.

Genomic DNA was extracted from overnight cultures using the DNeasy DNA Blood & Tissue Kit (Qiagen) according to the manufacturer's spin column protocol. Library preparation and whole-genome sequencing to a depth of ∼50x coverage was conducted at either the Max Planck Institute for Evolutionary Biology (Plön, Germany) or Eurofins Genomics (Constance, Germany) using Illumina MiSeq, NextSeq, or NovaSeq. The resulting reads were assembled against the reference *P. fluorescens* SBW25

genome (GenBank accession:AM181176.4) using the clonal option of Breseq (version 0.35.5) with default parameters [16]. Mutations were identified with breseq's HTML output and in the case of predicted novel junctions manually inspected with Geneious Prime. Marginal predictions were confirmed by Sanger sequencing. PCR products for Sanger sequencing were purified with EXOSAP and sequencing conducted by the Max Planck Insitute for Evolutionary biology, prepared using the BigDye Terminator v3.1 cycle sequencing kit followed by the BigDye XTerminator purification kit (ThermoFisher) according to manufacturer's instructions.

Strain construction

Isothermal Gibson Assembly reactions with the NEBuilder HiFi DNA Assembly master mix from New England BioLabs, were used for all molecular cloning procedures. Constructs to be integrated into the SBW25 genome contained flanking regions of 400-900 bp homologous to the site of integration and were assembled into the transfer plasmid pUISacB (accession pending). Primer overhangs were generated using the online NEBuilder tool (nebuilder.neb.com) and are available on request. All PCRs were performed using master mixes of high-fidelity polymerases (Phusion or Q5) and purified with the QIAquick PCR purification kit (Qiagen). pUISacB was extracted from overnight cultures using the QIAprep Spin Miniprep Kit (Qiagen), linearized with SpeI, amplified by PCR and digested with DpnI to remove remaining plasmid template. Assembled constructs were transformed into chemically competent *E. coli* Top 10 cells and integrated into SBW25 via two-step allelic exchange as previously described [2], but with final mutant selection using sucrose counter-selection on tryptone yeast extract and sucrose (TYS10) plates (10 g/L tryptone, 5 g/L yeast extract, 10% (w/v) filtered sucrose, 15 g/L agar).

For the *pflu0185* 'frame-shift detector' used to measure local frame-shift rate, a fusion was constructed with *kanR* via the linker sequence 'GCTAGCAGCGCAAGCGCAAGCGCA' (ASSASASA), such that the latter gene was 1bp out of frame with respect to *pflu0185* (an in-frame version of the same *kanR* fusion was also constructed). Three synonymous mutations engineered into the 5' end of *kanR* were required to remove aberrant start codons that existed in the out-of-frame sequence (which otherwise re-started the correct reading-frame). Strains expressing fluorescent proteins for use in fitness assays were constructed via standard conjugation of recipient SBW25 cells and *E. coli* donor containing pMRE-Tn*7*-145 (mScarlet-I) or pMRE-Tn*7*-152 (sGFP2) with media containing 0.1% w/v arabinose to induce Tn*7* transposase genes [48].

Transposon mutagenesis

Transposon mutagensis using Tn*5* was conducted according to the previously described method [22].

Briefly, this involved a tri-parental conjugation between the recipient CEL$^+$ and an *E. coli* donor containing the plasmid pCM639 with the IS-Ω-kan/hah transposon along with *E. coli* containing the helper plasmid pRK2013. Suppressor mutants were identified by screening for CEL$^-$ colonies. The site of insertion was determined by amplifying the transposon-chromosome junction through arbitrarily-primed PCR with Sanger sequencing of the resulting product.

Minimum inhibitory concentrations

Minimum inhibitory concentration (MIC), used as a proxy for transcription, was determined by plating $\sim 10^8$ cells of the relevant genotypes engineered with an in-frame *pflu0185*:*kanR* fusion onto KB agar and applying a kanamycin MIC test strip (Liofilchem). After 24 hours growth the MIC was determined by identifying where the margin of growth intercepted the strip in three independent replicates. In cases where genotypes exhibited high levels of resistance extending beyond the maximum measurable range of the test strips (256 μg ml^{-1}), the assay was instead conducted on agar containing either 100 or 200 μg ml^{-1} of kanamycin and the concentrations summed.

Fluctuation assays

Colony counts on selective and non-selective plates were used to estimate mutation rates using the rSalvador R package (v1.9), which generates a maximum likelihood estimate of mutation rate under the Luria-Delbruck model while accounting for variation in plating efficiency[62]. The likelihood ratio method was used to calculate confidence intervals and the statistical significance of differences between mutation rate estimates. Global mutation rates were assessed using rifampicin (100 μg ml^{-1}) and kanamycin (at concentrations of 10-50 μg ml^{-1} depending on *pflu0185* expression) used to determine rates of frame-shifting within *pflu0185*. Twelve independent cultures were used to determine spontaneous mutants; 6 were used to determine population size. To minimize confounding fitness differences between CEL$^-$and CEL$^+$states, all strains used for *pflu0185*frame-shifting fluctuation assays were modified with a cellulose inactivating mutation (WssEΔ993L-1260E) so that cells maintained the CEL$^-$state.

Fitness assays

Fitness was measured by 1:1 competition in either static (for CEL$^+$) or shaken (for CEL$^-$) microcosms. Shaking microcosms were used as a proxy environment for CEL$^-$due to difficulty of reconstituting the selective conditions of growth within a CEL$^+$mat. Competitors were fluorescently marked with either mScarlet-I or sGFP2 and were otherwise isogenic but for the secondary mutation of interest. The control consisted of a single representative CEL$^-$or CEL$^+$strain with both fluorescent markers competed against itself. Starting populations were derived from colonies inoculated into KB microcosms and grown 24 hours at 28°C in a shaking incubator. Microcosms were then vortexed and in the case of CEL$^+$ strains, sonicated (Bandelin Sonopuls mini 20; 2mm probe, 80% amplitude, 20 second duration) to further break up cell aggregates. Competitors were then mixed 1:1 and diluted in filtered PBS (0.22μM filter) with the initial ratio of fluorescent events obtained using flow cytometry (MACSQuant VYB). 6 μl of the 1:1 mix was also used to initiate competitions, which ran for either 24 (shaken) or 48 (static) hours. Following competitive growth, microcosms were vortexed (and static CEL$^+$ microcosms again sonicated), diluted in filtered PBS, and the final ratios determined by flow cytometry. Fitness was calculated as the ratio of Malthusian parameters [32].

Acknowledgements

The authors acknowledge generous core support from the Max Planck Society and thank members of the Department of Microbial Population Biology for help, ideas and discussion, and Alina Waldmann for genomic DNA purification. The authors are especially grateful to David Rogers for insight into the mechanism by which the HNrepeat achieves the first duplication and suggestion of a strategy for measuring frame-shift mutations. We are also indebted to Richard Moxon for valuable comment and discussion.

Author contributions

MB and PBR: experimental concept and design. MB: experimental work and analysis with technical assistance by LZ. MB and PBR wrote the paper.

Data availability

All data are available in Supplementary Information, can be explored at: https://micropop.evolbio.mpg.de/data/evolve and retrieved from Edmond https://doi.org/10.17617/3.5PEE52

References

[1] Amicone, M., Borges, V., Alves, M. J., Isidro, J., Zé-Zé, L., Duarte, S., Vieira, L., Guiomar, R., Gomes, J. P., and Gordo, I. Mutation rate of sars-cov-2 and emergence of mutators during experimental evolution. *Evolution, medicine, and public health 10*, 1 (2022), 142–155.

[2] Bantinaki, E., Kassen, R., Knight, C. G., Robinson, Z., Spiers, A. J., and Rainey, P. B. Adaptive divergence in experimental populations of pseudomonas fluorescens. III. mutational origins of wrinkly spreader diversity. *Genetics 176*, 1 (May 2007), 441–453.

[3] Bayliss, C. D., Field, D., Moxon, E. R., et al. The simple sequence contingency loci of haemophilus influenzae and neisseria meningitidis. *The Journal of clinical investigation 107*, 6 (2001), 657–666.

[4] Beaumont, H. J., Gallie, J., Kost, C., Ferguson, G. C., and Rainey, P. B. Experimental evolution of bet hedging. *Nature 462*, 7269 (2009), 90–93.

[5] Black, A. J., Bourrat, P., and Rainey, P. B. Ecological scaffolding and the evolution of individuality. *Nat Ecol Evol 4*, 3 (Mar. 2020), 426–436.

[6] Cai, Y.-M., Yu, K.-W., Liu, J.-H., Cai, Z., Zhou, Z.-H., Liu, Y., Wang, T.-F., and Yang, L. The c-di-gmp phosphodiesterase pipa (pa0285) regulates autoaggregation and pf4 bacteriophage production in pseudomonas aeruginosa pao1. *Applied and Environmental Microbiology 88*, 12 (2022), e00039–22.

[7] Canino-Koning, R., Wiser, M. J., and Ofria, C. Fluctuating environments select for short-term phenotypic variation leading to long-term exploration. *PLoS computational biology 15*, 4 (2019), e1006445.

[8] Colizzi, E. S., van Dijk, B., Merks, R. M., Rozen, D. E., and Vroomans, R. M. Evolution of genome fragility enables microbial division of labor. *Molecular Systems Biology 19*, 3 (2023), e11353.

[9] Conrad, M. Bootstrapping on the adaptive landscape. *Biosystems. 11*, 2-3 (Aug. 1979), 167–182.

[10] Couce, A., Caudwell, L. V., Feinauer, C., Hindré, T., Feugeas, J.-P., Weigt, M., Lenski, R. E., Schneider, D., and Tenaillon, O. Mutator genomes decay, despite sustained

fitness gains, in a long-term experiment with bacteria. *Proc. Natl. Acad. Sci. U. S. A. 114*, 43 (Oct. 2017), E9026–E9035.

[11] Crombach, A., and Hogeweg, P. Evolution of evolvability in gene regulatory networks. *PLoS computational biology 4*, 7 (2008), e1000112.

[12] Dasgupta, N., and Ramphal, R. Interaction of the antiactivator flen with the transcriptional activator fleq regulates flagellar number in pseudomonas aeruginosa. *Journal of bacteriology 183*, 22 (2001), 6636–6644.

[13] Datta, A., and Jinks-Robertson, S. Association of increased spontaneous mutation rates with high levels of transcription in yeast. *Science 268*, 5217 (1995), 1616–1619.

[14] Dawkins, R. The evolution of evolvability. In *Artificial life*. Routledge, 1989, pp. 201–220.

[15] De Bolle, X., Bayliss, C. D., Field, D., van de Ven, T., Saunders, N. J., Hood, D. W., and Moxon, E. R. The length of a tetranucleotide repeat tract in haemophilus influenzae determines the phase variation rate of a gene with homology to type III DNA methyltransferases. *Mol. Microbiol. 35*, 1 (Jan. 2000), 211–222.

[16] Deatherage, D. E., and Barrick, J. E. Identification of mutations in laboratory-evolved microbes from next-generation sequencing data using breseq. *Engineering and analyzing multicellular systems: methods and protocols* (2014), 165–188.

[17] Domínguez-Cuevas, P., and Marqués, S. Compiling sigma-70-dependent promoters. *Virulence and gene regulation* (2004), 319–343.

[18] Draghi, J., and Wagner, G. P. Evolution of evolvability in a developmental model. *Evolution 62*, 2 (2008), 301–315.

[19] Eshel, I. Clone selection and the evolution of modifying features. *Theoretical Population Biology 4*, 2 (1973), 196–208.

[20] Ferrare, J. T., and Good, B. H. Evolution of evolvability in rapidly adapting populations. *bioRxiv* (2023), 2023–07.

[21] Ganesan, A., Spivak, G., and Hanawalt, P. C. Transcription-coupled dna repair in prokaryotes. *Progress in molecular biology and translational science 110* (2012), 25–40.

[22] Giddens, S. R., Jackson, R. W., Moon, C. D., Jacobs, M. A., Zhang, X.-X., Gehrig,

S. M., and Rainey, P. B. Mutational activation of niche-specific genes provides insight into regulatory networks and bacterial function in a complex environment. *Proceedings of the National Academy of Sciences 104*, 46 (2007), 18247–18252.

[23] Graves, C. J., Ros, V. I., Stevenson, B., Sniegowski, P. D., and Brisson, D. Natural selection promotes antigenic evolvability. *PLoS pathogens 9*, 11 (2013), e1003766.

[24] Graves, C. J., and Weinreich, D. M. Variability in fitness effects can preclude selection of the fittest. *Annual review of ecology, evolution, and systematics 48* (2017), 399–417.

[25] Hammerschmidt, K., Rose, C. J., Kerr, B., and Rainey, P. B. Life cycles, fitness decoupling and the evolution of multicellularity. *Nature 515*, 7525 (Nov. 2014), 75–79.

[26] Hickman, J. W., and Harwood, C. S. Identification of fleq from pseudomonas aeruginosa as ac-di-gmp-responsive transcription factor. *Molecular microbiology 69*, 2 (2008), 376–389.

[27] Hogeweg, P. Toward a theory of multilevel evolution: long-term information integration shapes the mutational landscape and enhances evolvability. *Evolutionary systems biology* (2012), 195–224.

[28] Jinks-Robertson, S., and Bhagwat, A. S. Transcription-associated mutagenesis. *Annual review of genetics 48* (2014), 341–359.

[29] Kashtan, N., Noor, E., and Alon, U. Varying environments can speed up evolution. *Proc. Natl. Acad. Sci. U. S. A. 104*, 34 (Aug. 2007), 13711–13716.

[30] Kirschner, M., and Gerhart, J. Evolvability. *Proceedings of the National Academy of Sciences 95*, 15 (1998), 8420–8427.

[31] Lancaster, A. K., and Masel, J. The evolution of reversible switches in the presence of irreversible mimics. *Evolution 63*, 9 (2009), 2350–2362.

[32] Lenski, R. E., Rose, M. R., Simpson, S. C., and Tadler, S. C. Long-term experimental evolution in escherichia coli. i. adaptation and divergence during 2,000 generations. *The American Naturalist 138*, 6 (1991), 1315–1341.

[33] Leon, D., D'Alton, S., Quandt, E. M., and Barrick, J. E. Innovation in an e. coli evolution experiment is contingent on maintaining adaptive potential until competition subsides. *PLoS Genetics 14*, 4 (2018), e1007348.

[34] Lescat, M., Launay, A., Ghalayini, M., Magnan, M., Glodt, J., Pintard, C., Dion,

S., Denamur, E., and Tenaillon, O. Using long-term experimental evolution to uncover the patterns and determinants of molecular evolution of an escherichia coli natural isolate in the streptomycin-treated mouse gut. *Molecular ecology 26*, 7 (2017), 1802–1817.

[35] Levinson, G., and Gutman, G. A. Slipped-strand mispairing: a major mechanism for dna sequence evolution. *Molecular biology and evolution 4*, 3 (1987), 203–221.

[36] Lewontin, R. C. The units of selection. *Annual review of ecology and systematics 1*, 1 (1970), 1–18.

[37] Libby, E., and Rainey, P. B. Exclusion rules, bottlenecks and the evolution of stochastic phenotype switching. *Proceedings of the Royal Society B: Biological Sciences 278*, 1724 (2011), 3574–3583.

[38] Lind, P. A., Farr, A. D., and Rainey, P. B. Experimental evolution reveals hidden diversity in evolutionary pathways. *elife 4* (2015), e07074.

[39] Lynch, M. The frailty of adaptive hypotheses for the origins of organismal complexity. *Proceedings of the National Academy of Sciences 104*, suppl_1 (2007), 8597–8604.

[40] Moxon, E. R., Rainey, P. B., Nowak, M. A., and Lenski, R. E. Adaptive evolution of highly mutable loci in pathogenic bacteria. *Current biology 4*, 1 (1994), 24–33.

[41] Moxon, R., and Kussell, E. The impact of bottlenecks on microbial survival, adaptation, and phenotypic switching in host-pathogen interactions. *Evolution 71*, 12 (Dec. 2017), 2803–2816.

[42] Muriel, C., Arrebola, E., Redondo-Nieto, M., Martínez-Granero, F., Jalvo, B., Pfeilmeier, S., Blanco-Romero, E., Baena, I., Malone, J. G., Rivilla, R., and Martín, M. AmrZ is a major determinant of c-di-GMP levels in pseudomonas fluorescens F113. *Sci. Rep. 8*, 1 (Jan. 2018), 1979.

[43] Parter, M., Kashtan, N., and Alon, U. Facilitated variation: how evolution learns from past environments to generalize to new environments. *PLoS Comput. Biol. 4*, 11 (Nov. 2008), e1000206.

[44] Pepper, J. W. The evolution of evolvability in genetic linkage patterns. *Biosystems 69*, 2-3 (2003), 115–126.

[45] Pigliucci, M. Is evolvability evolvable? *Nature Reviews Genetics 9*, 1 (2008), 75–82.

[46] Rainey, P. B., and Rainey, K. Evolution of cooperation and conflict in experimental bacterial populations. *Nature 425*, 6953 (2003), 72–74.

[47] Rainey, P. B., and Travisano, M. Adaptive radiation in a heterogeneous environment. *Nature 394*, 6688 (1998), 69–72.

[48] Schlechter, R. O., Jun, H., Bernach, M., Oso, S., Boyd, E., Muñoz-Lintz, D. A., Dobson, R. C., Remus, D. M., and Remus-Emsermann, M. N. Chromatic bacteria–a broad host-range plasmid and chromosomal insertion toolbox for fluorescent protein expression in bacteria. *Frontiers in Microbiology 9* (2018), 3052.

[49] Simm, R., Morr, M., Kader, A., Nimtz, M., and Römling, U. Ggdef and eal domains inversely regulate cyclic di-gmp levels and transition from sessility to motility. *Molecular microbiology 53*, 4 (2004), 1123–1134.

[50] Smith, J. M., and Maynard-Smith, J. *The evolution of sex*, vol. 4. Cambridge University Press Cambridge, 1978.

[51] Sniegowski, P. D., Gerrish, P. J., Johnson, T., and Shaver, A. The evolution of mutation rates: separating causes from consequences. *Bioessays 22*, 12 (Dec. 2000), 1057–1066.

[52] Sniegowski, P. D., Gerrish, P. J., and Lenski, R. E. Evolution of high mutation rates in experimental populations of e. coli. *Nature 387*, 6634 (1997), 703–705.

[53] Sniegowski, P. D., and Murphy, H. A. Evolvability. *Current Biology 16*, 19 (2006), R831–R834.

[54] Spiers, A. J., Kahn, S. G., Bohannon, J., Travisano, M., and Rainey, P. B. Adaptive divergence in experimental populations of pseudomonas fluorescens. i. genetic and phenotypic bases of wrinkly spreader fitness. *Genetics 161*, 1 (May 2002), 33–46.

[55] Taddei, F., Radman, M., Maynard-Smith, J., Toupance, B., Gouyon, P.-H., and Godelle, B. Role of mutator alleles in adaptive evolution. *Nature 387*, 6634 (1997), 700–702.

[56] Vakulskas, C. A., Brady, K. M., and Yahr, T. L. Mechanism of transcriptional activation by pseudomonas aeruginosa exsa. *Journal of bacteriology 191*, 21 (2009), 6654–6664.

[57] Virgo, N., Agmon, E., and Fernando, C. Lineage selection leads to evolvability at large population sizes. In *Artificial Life Conference Proceedings* (2017), MIT Press One Rogers Street, Cambridge, MA 02142-1209, USA journals-info . . . , pp. 420–427.

[58] Wagner, G. P., and Altenberg, L. Perspective: complex adaptations and the evolution of evolvability. *Evolution 50*, 3 (1996), 967–976.

[59] Watson, R. A., Wagner, G. P., Pavlicev, M., Weinreich, D. M., and Mills, R. The evolution of phenotypic correlations and "developmental memory". *Evolution 68*, 4 (2014), 1124–1138.

[60] Williams, G. C. *Adaptation and natural selection: A critique of some current evolutionary thought*, vol. 61. Princeton university press, 1966.

[61] Woods, R. J., Barrick, J. E., Cooper, T. F., Shrestha, U., Kauth, M. R., and Lenski, R. E. Second-order selection for evolvability in a large escherichia coli population. *Science 331*, 6023 (2011), 1433–1436.

[62] Zheng, Q. rsalvador: an r package for the fluctuation experiment. *G3: Genes, Genomes, Genetics 7*, 12 (2017), 3849–3856.